Characterising the performance benefits of a 1/7th scale morphing rotor blade

DOI: 10.46932/sfjdv6n7-026

Received on: Jun 13th, 2025
Accepted on: Jul 4th, 2025

Mars Burke
PhD student in Rotary Morphing
Institution: Brunel University of London (BUL)
Address: Kingston Ln, Uxbridge, London, UB8 3PH
E-mail: mars.burke@brunel.ac.uk

Alvin Gatto
PhD in Aerospace Enginering
Institution: Brunel University of London (BUL)
Address: Kingston Ln, Uxbridge, London, UB8 3PH
E-mail: alvin.gatto@brunel.ac.uk

ABSTRACT

Rotary-wing aircrafts serve as indispensable components in the advancement of aviation, valued for their ability to operate in diverse and challenging environments without the need for conventional runways. This versatility makes them ideal for applications such as environmental conservation, precision agriculture, emergency medical support, and rapid-response operations in rugged terrains. However, although highly manoeuvrable, rotary-wing platforms generally have lower aerodynamic efficiency than fixed-wing aircraft. This study aims to improve aerodynamic performance by examining a 1/7th-scale rotor blade model equipped with a NACA0012 airfoil using CROTOR software. The analysis focuses on optimal spanwise locations for separating morphing and fixed blade sections at 85%, 90%, and 95% of the blade radius with up to +20 degrees of twist incorporated into the design. Key performance metrics assessed in this investigation include lift coefficient (C_L), drag coefficient (C_D), lift-to-drag ratio (C_L/C_D), Mach number, power, thrust coefficient, and Figure of Merit (FOM). Results indicate that the 0.90 r/R position is optimal for dividing the morphing and fixed sections, achieving a significant improvement of over 7% in both lift-to-drag ratio and FOM. These findings underscore the substantial impact on the overall performance of the rotor system and rotational aerodynamics that geometric modifications through the inclusion of a morphing capability can ultimately realise.

Keywords: Helicopter, Rotor Blade, Rotary Morphing, Rotational Aerodynamics, Twist Morphing, Adaptive Structures.

1 INTRODUCTION

Morphing technologies in aerospace engineering can be traced back to the inception of powered flight, exemplified by the Wright Flyer's pioneering use of 'wing warping' for roll control [1]. Broadly defined, morphing refers to the intentional alteration of a flying vehicle's geometric configuration to enhance its performance. Such modifications may serve a range of objectives, including extending operational flight envelopes [2], [3], refining aerodynamic load distributions [4], and mitigating noise and

vibrations [5], [6]. Over the past several decades, investigations in this domain have broadened appreciably, drawing upon advanced numerical analyses [7]-[13], high-fidelity computational simulations [14]-[18], and wind tunnel investigations [19]-[30]. Collectively, these combined efforts have demonstrated that morphing configurations can achieve levels of adaptability and performance surpassing those attainable by conventional, non-adaptive systems. However, rotorcraft platforms introduce distinct engineering hurdles stemming from their complex aerodynamic, structural, and aeroelastic environments. The rotating blades must operate effectively under varying flight states, blade loading conditions, and intricate blade–wake interactions, that increases the difficulty of achieving stability, control, and structural integrity, which is more challenging than in fixed-wing counterparts. As a result, the spectrum of morphing approaches adopted in rotorcraft remains notably constrained compared to the extensive range of techniques explored in fixed-wing applications [31]. Early investigations into rotary-wing morphing date back to the 1947 Kaman K-125 prototype, which employed servo flaps placed near the three-quarter blade radius to enable in-flight blade twisting [1]. Although this pioneering arrangement delivered measurable aerodynamic benefits, it also incurred increased drag penalties due to the exposure of mechanical components.

Over the past few decades, designs have incorporated trailing-edge flaps that function similarly to ailerons. These systems reduce vibration and improve rotor performance [32]-[35]. Léon et al. [36] investigated a Static Extended Trailing Edge (SETE) design that increased chord along a significant portion of the blade radius, yielding measurable reductions in power requirements, enhanced speed, higher operational altitudes, and improved load-carrying capacity. In addition to planform modifications, several studies have focused on out-of-plane transformations. Active twist concepts, enabled by piezoelectric actuators, have shown promise in reducing vibratory loads with minimal power input [36]. For instance, adjusting the blade twist distribution improved the rotor efficiency and hover performance, as demonstrated by Mach-scaled composite blades [37]. However, such aerodynamic gains often result in higher vibratory loads, underscoring the complexity of achieving an optimal balance between performance and structural demands.

Despite significant advancements in rotorcraft morphing research, much of the existing work remains concentrated in specific areas. The majority of studies have focused on noise and vibration control, whilst attention has also been paid to blade materials and manufacturing, load and fatigue analysis, and control systems and actuation mechanisms [1]. In contrast, the field of rotational aerodynamics which encompassing numerous subdomains such as wake and tip vortex control, multi-element airfoil integration, blade surface optimisation, active and passive flow control methodologies, and real-time shape adaptation, has garnered relatively limited focus. Among these, real-time morphing for shape modification is particularly underexplored in rotorcraft engineering. To address this gap, the present

study investigates the potential of real-time morphing within the context of rotational aerodynamics. A scaled model of a Sea King helicopter rotor blade is studied whilst incorporating positive twist angles at various cut-off sections along the span. This approach seeks to demonstrate tangible aerodynamic and performance benefits compared to a baseline model with no twist, thereby contributing valuable insights to the advancement of morphing technologies in rotary-wing systems.

2 DESIGN AND METHODOLOGY

2.1 ROTOR BLADE GEOMETRY

This study used a 1/7th-scale model of a Sea King helicopter rotor blade. The baseline configuration featured a NACA0012 airfoil profile, a rotor span of 1.24 meters, and a chord length of 0.065 meters (0.053R). Cut-off sections dividing the fixed and morphing parts on the rotor blade were located at 1.054 meters (0.85 r/R), 1.116 meters (0.90 r/R), and 1.178 meters (0.95 r/R). Each geometric configuration was subjected to positive twist angles, starting from the baseline and increasing linearly up to +20 degrees ($0° < \Phi_{tip} < +20°$). The twist angle progresses from the cut-off section, reaching its maximum value at the blade tip.

2.2 NUMERICAL METHOD

The aerodynamic modelling and simulations in this study were conducted using the CROTOR software package, developed by Mark Drela at MIT for the analysis and design of ducted and free-tip propellers, rotor blades, and windmills. CROTOR employs the Blade Element Method (BEM) and the Minimum Induced Loss (MIL) principle to optimise the design process. BEMT integrates momentum theory, which evaluates thrust and power, with blade element theory, which determines the distribution of aerodynamic forces along the blade span. For helicopter rotors, BEMT accounts for induced velocity through the rotor disk and aerodynamic forces resulting from blade motion. The trapezoidal rule is used to integrate these forces along the span, providing a precise estimate of rotor performance and aerodynamic efficiency. The coefficients of lift (C_L) and drag (C_D) are computed using the following equations, derived from a modified Blade Element Momentum (BEM) theory:

$$C_L \approx \frac{1}{S}\sum_{i=0}^{n-1}\left(\frac{1}{2}\rho\begin{pmatrix} V_{rel\{i\}}^2\, c_i c_{\{l,i\}} + \\ V_{rel\{i+1\}}^2\, c_{\{i+1\}} c_{\{l,i+1\}} \end{pmatrix}\frac{r_{i+1}-r_i)}{2}\right) \quad (1)$$

$$C_D \approx \frac{1}{S}\sum_{i=0}^{n-1}\left(\frac{1}{2}\rho\left(\begin{matrix}V_{rel\{i\}}^2\, c_i c_{\{d,i\}} + \\ V_{rel\{i+1\}}^2\, c_{\{i+1\}} c_{\{d,i+1\}}\end{matrix}\right)\frac{r_{i+1}-r_i)}{2}\right) \quad (2)$$

2.3 MACH-SCALED ANALYSIS

In this study, a Mach-scaled approach was adopted to study the morphing characteristics and aerodynamic performance of the rotor blade. This methodology was chosen to ensure that the critical compressibility effects observed in full-scale rotor operations, such as transonic shock formation were faithfully replicated in a scaled computational environment. The Mach number, as a defining parameter of compressible flow, directly influences the aerodynamic forces acting on the rotor blades at high speeds. The use of a Mach-scaled approach is particularly essential for investigating morphing blade configurations where changes in blade geometry; such as twist angles, alter the local flow characteristics and aerodynamic loads. Testing these configurations on full-scale blades is usually more time-intensive and operationally challenging, especially in the context of high-fidelity aerodynamic investigations or wind tunnel experiments. By maintaining Mach number similarity between the scaled model and full-scale rotor (i.e. Mach = 0.6), this study captured the key aerodynamic phenomena that govern rotor performance in operational scenarios of a full-scale rotor blade.

3 RESULTS AND DISCUSSION

3.1 EFFECTS OF POSITIVE TWIST ANGLES ON THE ROTOR BLADE AT 0.85 R/R

The changes in lift coefficient (ΔC_L) resulting from positive twist angles at a 0.85 r/R cut-off section between $0° \leq \Phi_{tip} \leq +20°$ are illustrated in Fig. 1 (a). From this figure, it is evident that increasing the positive twist angle leads to a higher lift coefficient. The largest increase in local C_L was found at the highest twist angle of +20° which corresponded to a rise of $\Delta C_L = 0.738$ at a spanwise location of r/R = 0.972 on the rotor blade. Incorporating lower, more fabrication-friendly twist angles (i.e. $+8° \leq \Phi_{tip} \leq +12°$) can still yield substantial aerodynamic benefits. For example, introducing a positive tip twist of +8° increases the lift coefficient by $\Delta C_L = +0.254$, an overall C_L increase of +9.7% for this configuration. The changes in aerodynamic efficiency ($\Delta\, C_L/C_D$) due to positive twist angles at a 0.85 r/R cut-off section are illustrated in Fig. 2. The maximum C_L/C_D value was found at $\Phi_{tip} = +18°$ whilst lower twist angles correspond to lower increases.

Figure 1

Effects of Changing Rotor Blade's Twist angle on Lift Coefficient (ΔC_L) at Cut-off Sections: (a) 0.85 r/R; (b) 0.90 r/R and (c) 0.95 r/R

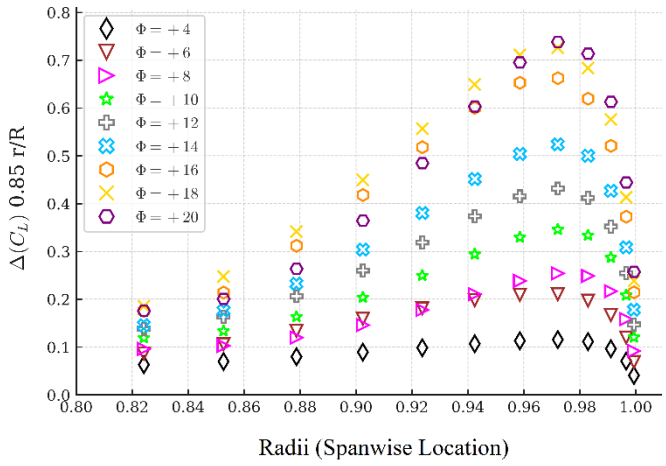

(a)

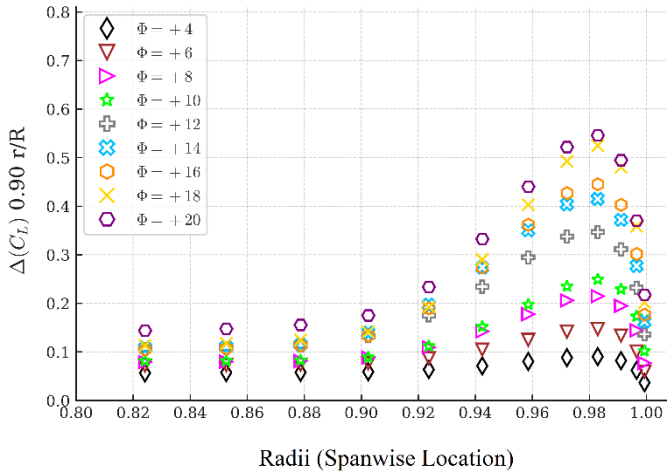

(b)

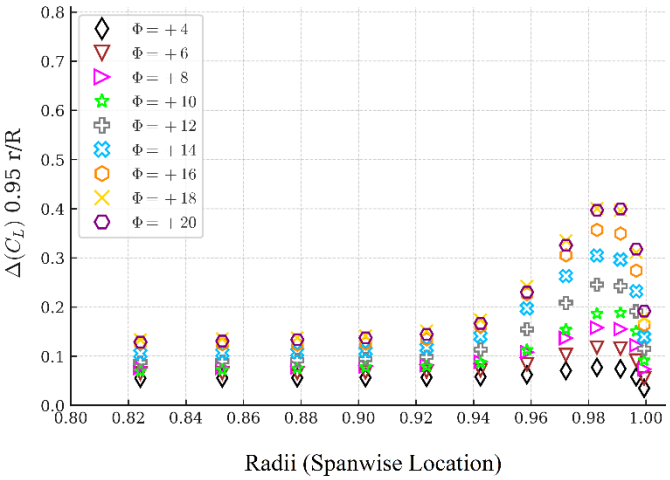

(c)

Figure 2

Effects of Changing Rotor Blade's Twist angle on Aerodynamic Efficiency (C_L/C_D) at 0.85 r/R, 0.90 r/R and 0.95 r/R cut-off sections

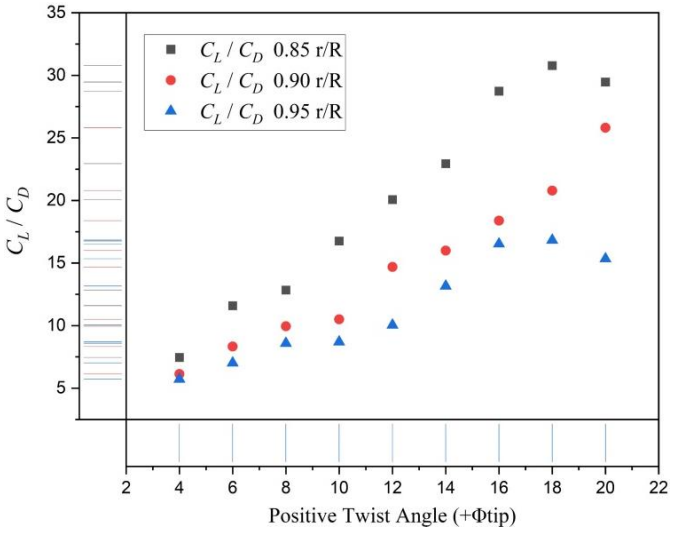

Extending the blade twist angle improved both the FOM and the thrust coefficient in hover normalised by the solidity ratio (C_{TH}/σ). The maximum increase in FOM was achieved at a twist angle of Φ_{tip} = +18°, corresponding to ΔFOM = + 0.2626. Even at a more moderate twist angle (Φ_{tip} = +8°), the FOM improved by ΔFOM = +0.125. A similar trend is observed for (C_{TH}/σ), with its maximum increment ($\Delta C_{TH}/\sigma$ = +0.0374) occurring at Φ_{tip} = +18° while the smaller twist angle of Φ_{tip} = +8° yielded an increase of $\Delta C_{TH}/\sigma$ = +0.0085. In addition, the power coefficient in hover normalised by the solidity ratio (C_{PH}/σ) also increases with higher twist angles (Figs. 3, 4).

3.2 EFFECTS OF POSITIVE TWIST ANGLES ON THE ROTOR BLADE AT 0.90 R/R

The impact of positive twist angles on the lift coefficient (ΔC_L) at the 0.90 r/R cut-off section for $0° \leq \Phi_{tip} \leq +20°$ is depicted in Fig. 1 (b). It is clear from the data that higher positive twist angles result in greater increases in lift coefficient. The maximum increase in local lift coefficient (ΔC_L = +0.545) occurred at the highest twist angle of Φ_{tip} = +20° measured at a spanwise location of r/R = 0.982. Adopting lower, more practical twist angles, such as $+8° \leq \Phi_{tip} \leq +12°$ could also achieve considerable aerodynamic gains. For instance, a positive tip twist of +8° resulted in an increase of ΔC_L = +0.214. The variations in aerodynamic efficiency ($\Delta C_L/C_D$) with positive twist angles at a 0.90 r/R cut-off section are shown in Fig. 2. The maximum C_L/C_D value is achieved at Φ_{tip} = +20°, while smaller increases are associated with lower twist angles. For example, introducing a tip twist of +8° enhances aerodynamic efficiency by $\Delta C_L/C_D$ = +3.83.

Both the FOM and the thrust coefficient in hover, normalised by the solidity ratio (C_{TH}/σ) demonstrated notable improvements with increases in blade tip twist angle. The highest increase in FOM (ΔFOM = +0.2311) was observed at a twist angle of Φ_{tip} = +20°. With a moderate twist angle of Φ_{tip} = +8°, the FOM achieved a noticeable increase of ΔFOM = +0.0995. Similarly, (C_{TH}/σ) reached its peak value ($\Delta C_{TH}/\sigma$ = +0.0229) at a positive twist angle of Φ_{tip} = +20°. While a smaller twist of Φ_{tip} = +8° still provided a measurable increase of $\Delta C_{TH}/\sigma$ = +0.0061 (Figs. 3, 4).

Figure 3

Effects of Changing Rotor Blade's Twist angle on FOM and (C_{TH}/σ) at 0.85 r/R, 0.90 r/R and 0.95 r/R cut-off sections with Positive Twist Angles up to 20º (+Φ_{tip})

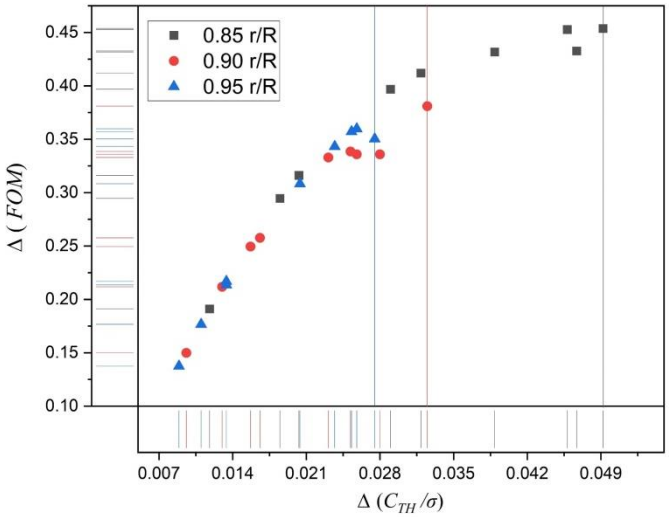

Figure 4

Effects of Changing Rotor Blade's Twist angle on (C_{TH}/σ) and (C_{PH}/σ) at 0.85 r/R, 0.90 r/R and 0.95 r/R cut-off sections with Positive Twist Angles up to 20º (+Φ_{tip})

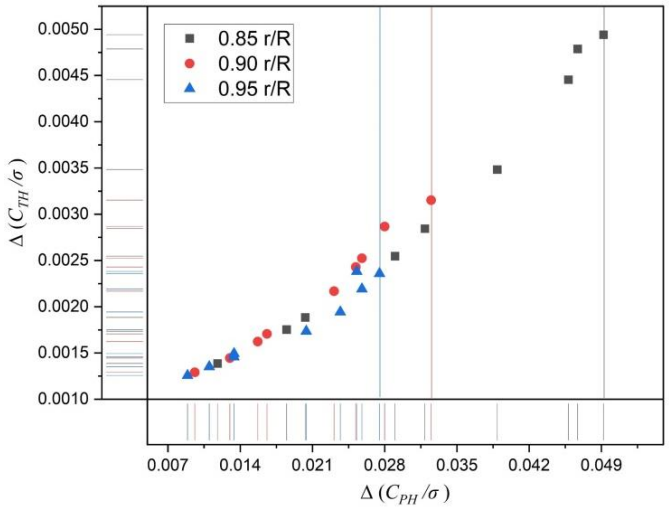

3.3 EFFECTS OF POSITIVE TWIST ANGLES ON THE ROTOR BLADE AT 0.95 R/R

The changes in lift coefficient (ΔC_L) resulting from positive twist angles at a 0.95 r/R cut-off section between $0° \leq \Phi_{tip} \leq 20°$ are illustrated in Fig. 1 (c). From this figure, it is evident that increasing the positive twist angle leads to a higher lift coefficient. The largest increase in local C_L was found at the highest twist angle of 20° which corresponded to a rise of $\Delta C_L = 0.3993$ at a spanwise location of r/R = 0.991 on the rotor blade. Incorporating lower, more fabrication-friendly twist angles (i.e. $8° \leq \Phi_{tip} \leq 12°$) can still yield substantial aerodynamic benefits. For example, introducing a positive tip twist of +8° increases the lift coefficient by $\Delta C_L = 0.157$. The changes in aerodynamic efficiency ($\Delta\ C_L/C_D$) due to positive twist angles at a 0.95 r/R cut-off section between are illustrated in Fig. 2. The maximum C_L/C_D value occurs at $\Phi_{tip} = 18°$ whilst lower twist angles correspond to lower increases. For example, a positive tip twist of +8° increases the aerodynamic efficiency by $\Delta\ C_L/C_D = 2.87$.

Figure 5

CROTOR's Output Illustrating the Aerodynamics, Rotor and Helicopter Performance Parameters at a 0.85 r/R Cut-off Section with a Positive Twist Angle of 20º (+Φ_{tip})

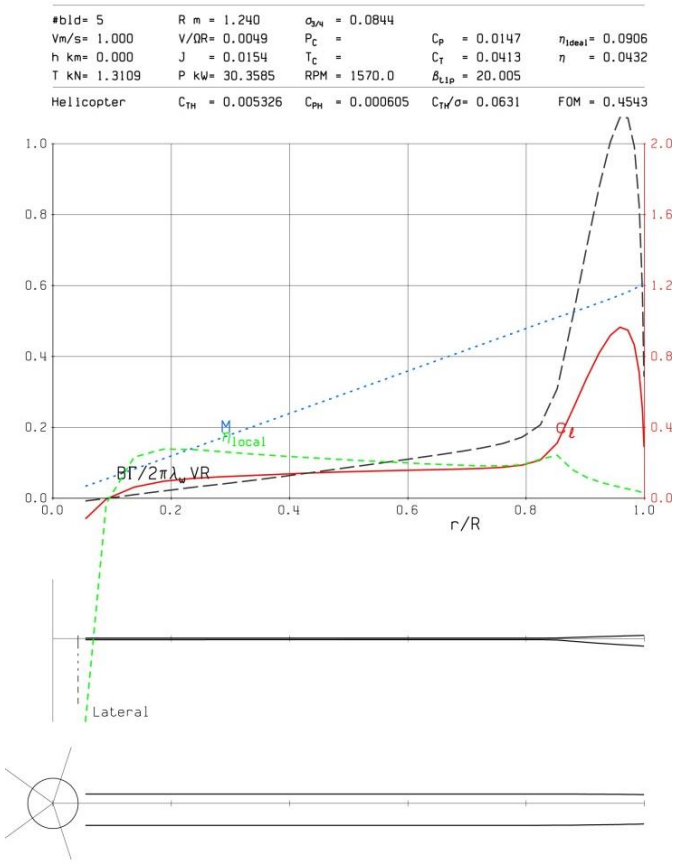

Figure 6

Acoustic Signature Created by the Rotor Blade Under Conditions set from Fig. 5

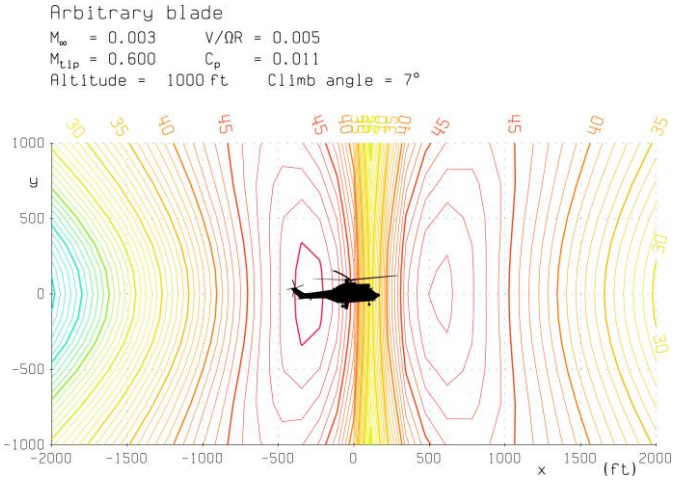

An increase in the blade twist angle positively influenced both the FOM and the thrust coefficient in hover, normalised by the solidity ratio (C_{TH}/σ). The largest increase in FOM, was observed at a positive twist angle of Φ_{tip} = +16° corresponding to ΔFOM = + 0.2222. Lower twist angles (i.e. Φ_{tip} = 8°) correspond to a ΔFOM increase of + 0.0794. The thrust coefficient in hover's maximum increase was shown to be at a twist angle (Φ_{tip} = 20°) with an associated Δ C_{TH}/σ = + 0.0186. This increase for a twist angle of Φ_{tip} = 8° was 0.0045 (Figs. 3, 4).

3.4 MACH NUMBER AND ACOUSTIC SIGNATURE

The aerodynamic environment for this scaled numerical assessment was governed by the baseline Mach-scaled condition (i.e. Mach ≈ 0.6). As illustrated in Fig. 5, the Mach number remains effectively unchanged, even at the most geometrically demanding configuration, namely; a +20° twist angle combined with a 0.85 r/R cut-off section. Even under these conditions, the design can capitalise on improvements in both C_L/C_D and the FOM (FOM) without approaching transonic tip speeds or precipitating shock formation. Furthermore, as shown in Fig. 6, this severe configuration does not adversely affect the acoustic signature, thereby mitigating concerns regarding increased noise levels.

4 CONCLUSIONS

This study has demonstrated and thoroughly characterised the performance improvements of a scaled morphing rotor blade in comparison to a conventional baseline configuration through the assessment of helicopter and rotorcraft performance parameters and aerodynamic coefficients. The

advantages of this design were presented, with both C_L/C_D and the FOM showing consistent enhancements across all cases. The 0.90 r/R configuration with low-to-moderate twist angles (i.e. $8° \leq \Phi_{tip} \leq 12°$) seem to be the most benefit-to-cost candidate by maintaining a balance between aerodynamic performance and design feasibility whilst achieving increases in C_L/C_D and FOM exceeding 7%. These findings underscore the significance of real-time adaptive structures and morphing designs in the relatively unexplored domain of rotary-wing aerodynamics and rotorcraft morphing, opening new avenues for innovative and transformative advancements in aerospace engineering.

REFERENCES

[1] Concilio, A., Dimino, I., Lecce, L., & Pecora, R. (2018). *Morphing wing technologies: Large commercial aircraft and civil helicopters.* Cambridge, MA: Butterworth-Heinemann.

[2] Mistry, M., & Gandhi, F. (2014). Helicopter performance improvement with variable rotor radius and RPM. *Journal of the American Helicopter Society*, *59*. https://doi.org/10.4050/JAHS.59.042010

[3] Buter, A., Ehlert, C., Sachau, U. D., & Breitbach, E. (2000, May 8–11). Adaptive rotor blade concepts: Direct twist and camber variation. In *RTO AVT Symposium on Active Control Technology for Enhanced Performance Operational Capabilities of Military Aircraft, Land Vehicles and Sea Vehicles*, Braunschweig, Germany.

[4] Arnold, U. (2003, September 16–18). Recent IBC flight test results from the CH-53G helicopter. In **29th European Rotorcraft Forum**, Friedrichshafen, Germany.

[5] Splettstoesser, W. R., Schultz, K.-J., Kube, R., Brooks, T. F., Booth Jr., E. R., Niesl, G., & Streby, O. (1994). A higher harmonic control test in the DNW to reduce impulsive BVI noise. *Journal of the American Helicopter Society*, *39*(4), 3–13.

[6] Brooks, T. F., & Booth Jr., E. R. (1993). The effects of higher harmonic control on blade-vortex interaction noise and vibration. *Journal of the American Helicopter Society*, *38*(3), 45–55.

[7] Barbarino, S., Ameduri, S., & Pecora, R. (2007, July 1–4). Wing chamber control architectures based on SMA: Numerical investigations. In Du, S., Leng, J., & Asundi, A. K. (Eds.), *Proceedings of SPIE International Conference on Smart Materials and Nanotechnology in Engineering (SMN2007)* (Vol. 6423, p. 64231E), Harbin, China.

[8] Le Pape, A. (2005). Numerical aerodynamic optimization of helicopter rotors: Multi-objective optimization in hover and forward flight conditions. In *Proceedings of the 31st European Rotorcraft Forum*, Florence, Italy.

[9] Duri, S. (2013, September 9–12). A leading edge morphing architecture for droop nose effect. In *XXII AIDAA National Congress*, Napoli, Italy.

[10] Meduri, S. (2014, July 18–19). A SMA-based morphing leading edge architecture. In *The 5th International Conference on Mechanical and Aerospace Engineering (ICMAE 2014)*, Madrid (Best Conference Oral Presentation Award).

[11] Barbarino, S., Pecora, R., Lecce, L., Concilio, A., Ameduri, S., & De Rosa, L. (2011). Airfoil structural morphing based on SMA actuator series: Numerical and experimental studies. *Journal of Intelligent Material Systems and Structures*, *22*(10), 987–1004

[12] Arena, M., Noviello, M. C., Rea, F., Amoroso, F., Pecora, R., & Amendola, G. (2016). Modal stability assessment for a morphing aileron subjected to actuation system failures: Numerical analysis supported by test evidence. In *Proceedings of the 7th International Conference on Mechanical and Aerospace Engineering (ICMAE 2016)* (pp. 437–442).

[13] Botez, R. M., Koreanschi, A., Gabor, O. S., Mebarki, Y., Mamou, M., Tondji, Y., Amoroso, F., Pecora, R., Lecce, L., Amendola, G., Dimino, I., & Concilio. (2017). Numerical and experimental testing of a morphing upper surface wing equipped with conventional and morphing ailerons. In *55th AIAA Aerospace Sciences Meeting* (January 9–13, 2017, Grapevine, TX).

https://doi.org/10.2514/6.2017-0445

[14] Cambier, L., Heib, S., & Plot, S. (2013). The ONERA elsA CFD software: Input from research and feedback from industry. *Mécanique & Industries, 14*, 159–174.

[15] Destarac, D. (2003). Far-field/near-field drag balance and applications of drag extraction in CFD. In *VKI Lecture Series CFD Based Aircraft Drag Prediction and Reduction*, Hampton, VA.

[16] Dumont, A., & Carrier, G. (2014, July). Multi-point aerodynamic optimization of a flexible transport aircraft wing using an aeroelastic adjoint method. In *6th European Conference on Computational Fluid Dynamics (ECFD VI)*, Barcelona, Spain.

[17] Waller, G. (2002, September 8–13). CFD prediction of stability derivatives of a turboprop aircraft using a Cartesian grid-based Euler code. In *23rd International Congress of Aeronautical Science (ICAS 2002)*, Toronto, Canada.

[18] Boyd Jr., D., & Douglas, D. (2009, September 22–25). Aerodynamic and acoustic study of an active twist rotor using a loosely coupled CFD/CSD method. In *Proceedings of the 35th European Rotorcraft Forum* (Article 1160), Hamburg, Germany.

[19] Bartley-Cho, J. D., Wang, D. P., Martin, C. A., Kudva, J. N., & West, M. N. (2004). Development of high-rate, adaptive trailing edge control surface for the Smart Wing Phase 2 wind tunnel model. *Journal of Intelligent Material Systems and Structures, 15*, 279–291.

[20] Guiler, R., & Huebsch, W. (2005, June 6–9). Wind tunnel analysis of a morphing swept tailless aircraft. In *Proceedings of the 23rd AIAA Applied Aerodynamics Conference* (AIAA 2005-4981, 14 pp.), Toronto, Ontario, Canada.

[21] Kim, D. K., Han, J. H., & Kwon, K. J. (2009). Wind tunnel tests for a flapping wing model with a changeable camber using macro-fiber composite actuators. *Smart Materials and Structures, 18*, 024008.

[22] Neal, D. A., Farmer, J., & Inman, D. J. (2006, May 1–4). Development of a morphing aircraft model for wind tunnel experimentation. In *Proceedings of the 47th AIAA/ASME/ASCE/AHS/ASC Structures, Structural Dynamics, and Materials Conference* (AIAA 2006-2141), Newport, RI

[23] Ruggeri, R. T., Arbogast, D. J., & Bussom, R. C. (2008, April 7–10). Wind tunnel testing of a lightweight ¼-scale actuator utilizing shape memory alloy. In *Proceedings of the 49th AIAA/ASME/ASCE/AHS/ASC Structures, Structural Dynamics, and Materials Conference* (AIAA 2008-2279), Schaumburg, IL.

[24] Straub, F., Anand, V. R., Birchette, T., & Lau, B. H. (2009, September 22–25). SMART rotor development and wind tunnel test. In *Proceedings of the 35th European Rotorcraft Forum (ERF 2009)* (Article 1200, 21 pp.), Hamburg, Germany.

[25] Studebaker, K., & Matuska, D. (1993, May). Variable diameter tiltrotor wind tunnel test results. In *Proceedings of the American Helicopter Society 49th Annual Forum*, St. Louis, MO.

[26] Wang, D. P., Bartley-Cho, J. D., Martin, C. A., & Hallam, B. J. (2001, March 5–8). Development of high-rate, large deflection, hingeless trailing edge control surface for the Smart Wing wind tunnel model. In *Proceedings of SPIE Smart Structures and Materials 2001: Industrial and Commercial Applications of Smart Structures Technologies* (Vol. 4332, pp. 407–418), Newport Beach, CA.

[27] Popov, A. V., Grigorie, T. L., Botez, R. M., Mamou, M., & Mebarki, Y. (2010, July–August). Closed-loop control validation of a morphing wing using wind tunnel tests. *Journal of Aircraft, 47*(4), 1309–1317.

[28] Noboru, K., & Saito, S. (2008, April 29–May). Performance evaluation of full-scale on-board active flap system in transonic wind tunnel. In *64th American Helicopter Society Forum*, Montreal, Quebec, Canada.

[29] Woods, B., Wereley, N., & Kothera, C. (2010, September 28–October 1). Wind tunnel testing of a helicopter rotor trailing edge flap actuated via pneumatic artificial muscles. In *ASME 2010 Conference on Smart Materials, Adaptive Structures and Intelligent Systems*, Philadelphia, PA.

[30] Berry, B., & Chopra, I. (2011, May 3–5). Wind tunnel testing for performance and vibratory loads of a variable-speed Mach-scale rotor. In *67th American Helicopter Society Forum*, Virginia Beach, VA

[31] Barbarino, S., Bilgen, O., Ajaj, R. M., Friswell, M. I., & Inman, D. J. (2011). A review of morphing aircraft. *Journal of Intelligent Material Systems and Structures*, 22, 823–877.

[32] Straub, F., Anand, V., Birchette, T., & Lau, B. (2009). SMART rotor development and wind tunnel test. In *35th European Rotorcraft Forum*, Hamburg, Germany.

[33] Dietrich, O., Enenkl, B., & Roth, D. (2006). Trailing edge flap for active rotor control: Aeroelastic characteristics of the ADASYS rotor system. In *62nd American Helicopter Society Forum*, Phoenix, AZ.

[34] Roth, D., Enenkl, B., & Dietrich, O. (2006, September). Active rotor control by flaps for vibration reduction: Full-scale demonstrator and first flight results. In *32nd European Rotorcraft Forum*, Maastricht, The Netherlands.

[35] Léon, O., & Gandhi, F. (2009). Rotor power reduction using multiple spanwise-segmented, optimally-actuated trailing-edge flaps. In *35th European Rotorcraft Forum (ERF 2009)* (Vol. 1, pp. 431–445).

[36] Léon, O., Hayden, E., & Gandhi, F. (2009). Rotorcraft Operating Envelope Expansion Using Extendable Chord Sections. Presented at the American Helicopter Society 65th Annual Forum, Grapevine, Texas, May 27–29, 2009.

[37] Bao, Jinsong & Nagaraj, V.T. & Chopra, Inderjit & Bernhard, A.P.F.. (2003). Design and Hover Test of Low Vibration Mach Scale Rotor with Twisted Composite Tailored Blade. Collection of Technical Papers - AIAA/ASME/ASCE/AHS/ASC Structures, Structural Dynamics and Materials Conference. 5. 10.2514/6.2003-1787.

NOMENCLATURE

BEM/T = Blade element method/theory
CROTOR = MIT's numerical Code for design and analysis of rotary ducted and free-tip propellers and windmills
FOM = figure of merit (ratio of the ideal power to actual power) $C_{TH}^{3/2} / C_{PH}\sqrt{2}$
MIL = minimum induced loss
RPM = rotations per minute
C_D, C_L, C_P, C_{PH}, C_T, C_{TH} = rotor's drag, lift, power, power in hover, thrust, thrust in hover coefficients
C_L / C_D = rotor's aerodynamic efficiency
σ = ratio of the total rotor blade area to the total disc area (solidity ratio)
C_{TH} / σ = rotor coefficient of thrust in hover to rotor solidity ratio
c = chord (m)
μ = advance ratio (ratio of the forward speed of the helicopter to the speed of the rotor blade tip)
T = thrust (N)
P = power (W)
M = Mach number
v_i = freestream velocity (m/s)
nn r/R = cut-off spanwise section/ rotor radius
$+\Phi_{tip}$ = linear positive (wash-in) geometrical twist at the rotor blade's tip
ρ = density (kg/m^3)